Integration of Coseismic Deformation into WebGIS for Near Real-time Disaster Evaluation and Emergency Response

Rui Zhao[1], Xintao Liu[1, *], Wenbin Xu[2, 3, *]

[1] Department of Land Surveying and Geo-Informatics, The Hong Kong Polytechnic University, Kowloon, Hong Kong

[2] School of Geosciences and Info-Physics, Central South University, Changsha 410083, Hunan, China.

[3] Key Laboratory of Metallogenic Prediction of Nonferrous Metals and Geological Environment Monitoring (Central South University), Ministry of Education, Changsha 410083, Hunan, China.

Abstract

Earthquakes are one of the destructive natural disasters. Immediate emergency response in the first few hours is important for life rescue. The near real-time ground deformation maps generated after earthquakes are crucial for hazard assessments, which normally take a couple of hours or longer to be generated using conventional ways. In this study, we propose a near real-time coseismic ground deformation map generation system with the aim of assisting rapid seismic hazard evaluations and emergency responses. This framework adopts the source parameters published by seismological agencies and uses the empirical equations to generate the near real-time coseismic ground deformation maps. The source parameters of an earthquake, such as the focal mechanism, are programmatically accessed from the United States Geological Survey National Earthquake Information Center (USGS-NEIC) in a nearly real-time manner. The ground deformation estimated using empirical equations is integrated as self-adapting spatial data fusion and visualized on an interactive WebGIS platform. We developed the WebGIS platform, namely QuickDeform at www.insar.com.cn, and successfully applied the system to several recent large magnitude earthquakes. We observed that the proposed framework functions robustly and proficiently to automatically generate the seismic deformation map within several minutes after the occurrence of an earthquake. The generated deformation map shows good agreement when compared to the data from real earthquakes. QuickDeform can be used as a volunteered geographic information platform for crowdsourcing disaster data for rescue and model validation.

Keywords: Coseismic deformation, Real-time WebGIS, Earthquake modeling, Hazard assessment

1. Introduction

With the development of science and technology, enormous achievements have been made in the field of seismology (Douglas & Edwards, 2016). The large magnitude earthquakes often lead to huge economic losses and massive casualties. In the contemporary world, due to the rapid development of hardware technology, seismic monitoring became feasible. The Global Seismographic Network (GSN), which is collectively built by the USGS-NEIC, National Science Foundation (NSF) and Incorporated Research Institutions for Seismology (IRIS) can provide near-uniform, worldwide monitoring, with over 150 modern seismic stations distributed globally (USGS-NEIC, 2018). As soon as an earthquake occurs, the seismic monitoring station will issue a warning and obtain valuable information from the seismic wave, such as location, magnitude, and focal mechanism (Vince, 2010). The seismic information provided by seismic stations can be used to study slip models (Hough & Susan, 2016) or to design and develop earthquake early warning systems (Wu et al., 1998).

Although much research is devoted in the study of seismic warnings, it is still difficult to achieve pre-seismic predictions and warnings, because of the uncertainty of the earthquake. Therefore, post-seismic disaster assessment and response play a major role in earthquake rescue. In 1992, a project called the Global Seismic Hazard Assessment Program (GSHAP) was launched by the International Council of Scientific Union (ICSU), resulting in the Global Seismic Hazard Map in 1999 (Giardini et al., 1999). To understand earthquakes and their associated hazards, certain studies focus on fault models to estimate seismic deformation (Xu et al., 2018). Although the abovementioned studies show that the seismic deformation patterns are considerably similar and accurate, this kind of study needs comprehensive research and constant adjustment of seismic parameters, which makes it difficult to obtain timely deformation results.

Interferometric synthetic aperture radar (InSAR) technology has been successfully used to study earthquake cycle deformation (Simons et al., 2002; Xu et al., 2015; Liu & Xu, 2019). However, due to its limited revisit time, these data cannot provide much useful information for seismic warnings. A rapid, efficient, and real-time earthquake disaster evaluation system plays a crucial role in seismic research and rescue. ShakeMap (Wald et al., 2019) is an automatic online seismic emergency tool designed to estimate motions in space area depending on the distance and seismic information from the earthquake and the rock and soil conditions at sites. Although this is a tool that can provide near real-time or real-time maps of ground motion and shaking intensity following significant earthquakes, it is not accurate enough for large-scale classification. ShakeMap provides coarse results by generating intensity contours which can only present large area ground motion without specific deformation value. The terms “near real-time” and “real-time” are different. Real-time responses are within seconds, whereas near real-time responses vary from seconds to minutes (Standard, 1996).

Numerous studies have investigated ground deformation and the geometrical complexity of faults (Beeler et al., 2001; Watson et al. 20Xu et al., 2018) and established an earthquake evaluation system and real-time or near real-time response (Atkinson & Boore, 1998; Allstadt et al., 2018). However, few of them are dedicated to proposing a framework that can integrate seismic deformation with GIS for real-time or near real-time disaster evaluation, visual analytics, and emergency response, even if such earthquake data are available. Therefore, the timely and precise response is of great importance in rescue operations. For instance, when an earthquake occurs near urban or rural areas, decision-makers and rescuers need to draw conclusions within several hours or even minutes. This study fills this research gap by proposing the integration of seismic deformation into WebGIS for real-time disaster evaluation and emergency response. We apply Okada rectangular dislocation model (Okada, 1985, 1992) and empirical

equations of fault to develop a framework that allows us to 1) automatically monitor the release of seismic information and access real-time seismic parameters of the earthquake; 2) simulate seismic deformation, and 3) generate self-adapting seismic deformation maps and integrate them on an interactive WebGIS platform.

The remainder of this paper is organized as follows: section 2 introduces related studies of earthquake early warning and seismic deformation analysis. Section 3 presents the methodology of our proposed framework, including the generation of seismic deformation maps and spatial data fusing. Section 4 shows certain implementation results generated from the developed platform, namely QuickDeform. Finally, we discuss performance and potential improvements. Section 5 summarizes the contributions and limitations of this study.

2. Related work

Researchers have focused on the early warning of earthquakes for a long time. In ancient China, people used seismographs to monitor the occurrence of earthquakes (Lin et al., 2019). Nowadays, people are using social media (e.g., Twitter) to broadcast essential earthquake information (Lacassin et al., 2019). This information can help the public understand the earthquake; however, for scientists, limited information is far from enough. To further study the occurrence of an earthquake, scientists would share their results of the latest earthquake research (Lacassin et al., 2019). However, the complexity of seismic deformation information analysis results in the lag of information. In this section, we introduce several cases of earthquake analysis to understand the research status.

In 1999, Wald et al. (1999) began studying the rapid earthquake warning system for earthquake analysis in California. They have developed the ShakeMap platform (https://earthquake.usgs.gov/data/shakemap/) more than 20 years ago, which is now applied to global earthquake warning (Wald et al., 2019). They use local geology, earthquake location, and magnitude to estimate shaking variations interpolated onto a rectangular grid uniformly sampled at a spacing interval of approximately 1.5 km. The results are divided into 10 levels, from I to X+. In addition, Kohler et al. (2020) improved the ShakeAlert, which uses the information collected from seismic stations and can deliver earthquake warning information, including earthquake source and ground motion, from ShakeMap to the public. Although they can respond within 3 to 5 min, the results for ground motion estimation are too coarse, with only 10 levels.

For geophysicists, more accurate surface deformation data can contribute to the better understanding of earthquake mechanisms. Consequently, InSAR is widely used to generate seismic deformation maps (Hu et al. 2012). Conventional InSAR technology can only measure one-dimensional deformation of the surface (Goldstein et al. 1988). Taking the 2003 Bam (Iran) earthquake as an example, Hu et al. (2010) presented a method to estimate three-dimensional surface deformation by combining SAR interferometric phase and amplitude information of ascending and descending orbits. They compared their results with simulated 3D co-seismic surface displacement field based on the Okada model and found that the displacement field corresponds well with the location of the fault with maximal displacement and can be used to generate reliable and highly accurate 3D surface displacement fields. Although the whole-day surface deformation cannot be detected due to the revisiting period mentioned before in this paper, it has great reference value for this paper.

3. Methodology

The main objective of this study is to integrate near real-time seismic deformation into an interactive WebGIS platform to evaluate earthquake disaster for immediate emergency response. This is a user-oriented GIS service, which supports viewing, searching, and customizing the seismic deformation, so that the near real-time disaster evaluation is significantly helpful for the earthquake rescue. This section presents the details about the methodology of our established platform.

3.1 Forward modeling

The Okada model, which is one of the most popular dislocation models, can describe the geometric and kinematic characteristics of faults in three dimensions and can calculate surface deformation by using the focal mechanism (Okada, 1985). Therefore, we selected the Okada model as our forward model (Fig. 1).

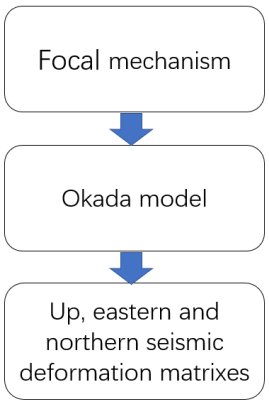

Figure 1. Okada model with the focal mechanism to calculate the seismic deformation.

For the earthquake rupture length and width estimates, we apply empirical equations of the scaling relations for moment magnitude and length/width which were derived based on a large dataset and can be expressed as (Blaser et al., 2010) follows:

$$L = 10^{0.57 \times Mw - 2.37} \quad (1)$$

$$W = 10^{0.46 \times Mw - 1.86} \quad (2)$$

where L is rupture length, W is the width, and Mw is moment magnitude. Due to the automatic process, the model should adapt to different depths of epicenters. In the original model, the epicenter is located in the middle of the geometric center of the fault. However, when an earthquake occurs at shallow depths, the actual epicenter location will be deeper than the model epicenter. This means that part of the fault model will break out of the surface, losing its effect. Therefore, we have improved the model. When the fault breaks out of the surface, we move the epicenter of the model to the center of the top edge of the fault. Through this forward modeling, we can gain the 3D surface displacement (i.e., northern, east, and up).

3.2 Coseismic ground deformation generation

We can project the simulated 3D displacement into the radar line of sight (LOS) displacement to synthesize an interferogram, which can be compared with the real InSAR data. The relationship $\triangle R$

between 3D surface displacements and the displacement in the LOS direction can be expressed as (Fialko et al., 2001) follows:

$$[-\sin\theta\cos\alpha \quad \sin\theta\sin\alpha \quad \cos\theta]\begin{bmatrix} uE \\ uN \\ uZ \end{bmatrix} = [\Delta R] \tag{3}$$

where θ represents the pixel-based radar incidence angle at the reflection point, α represents the orbit azimuth angle of the satellite heading vector (positive clockwise from North), uE is the deformation in the eastern direction, uN is the deformation in the northern direction, and uZ is the deformation in the vertical direction.

Moreover, the framework needs to simulate ascending and descending orbit deformations, and hence, we propose two group parameters (Table 1).

Table 1. Ascending and descending parameters

	θ (°)	α (°)
Ascending orbit	34	-14
Descending orbit	34	193

3.3 Automatic processing

The automation procedure is a crucial part of the framework, wherein the key to automation is time-effective. Initially, the focal mechanism provided by the USGS-NEIC lags when an earthquake happens, usually by a few dozen minutes. This happens because it takes time from monitoring an earthquake and calculating its magnitude and depth to calculating its focal mechanism. However, certain small or insignificant earthquakes do not have the focal mechanism. In addition, to make the framework more reasonable, the automated accessing data program should sleep for 5 to 10 min for the crawler technology.

The whole automated workflow (Fig. 2) of seismic surface deformation creates different types of deformation maps. Furthermore, if the earthquake is a new one, seismic parameters are stored in the resultant maps that can be obtained from forward modeling.

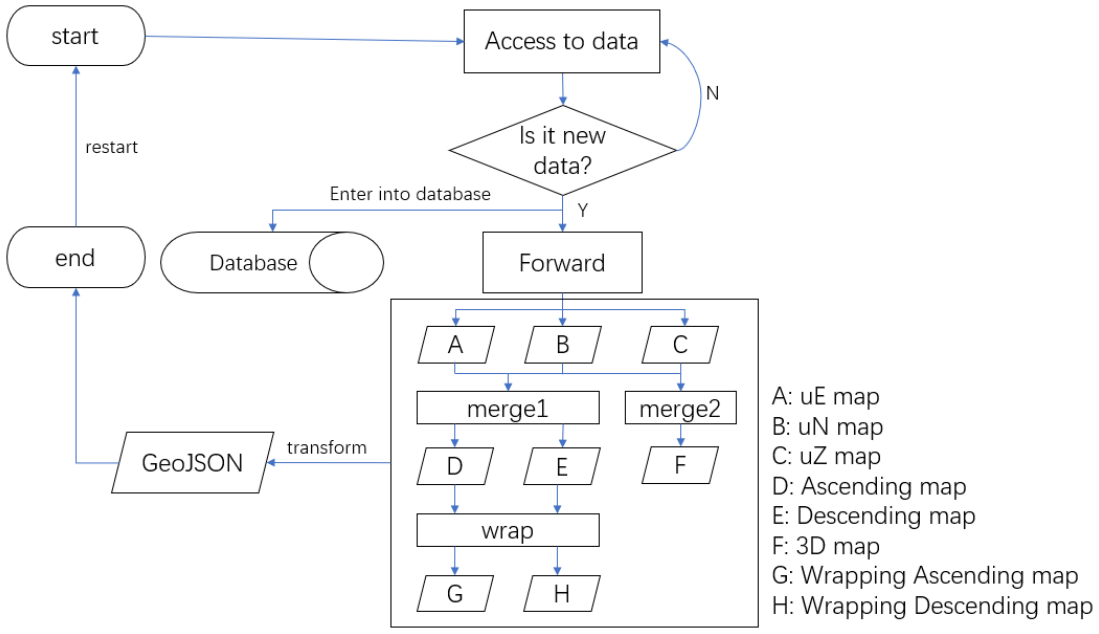

Figure 2. Data workflow

Through forward modeling, we first gain three surface displacement matrices that represent eastern, northern, and up to surface displacements, respectively. In addition, we can visualize them as uE, uN and uZ maps (Fig. 3 a, b, c). Afterward, we merge these three surface displacement matrices to simulate ascending and descending LOS by Eq. (3). After visualization, they become ascending and descending maps (Fig. 3 e, f). Another merging process is used for the 3D map (Fig. 3 e). Arrows represent horizon deformation, whose lengths represent size and directions represent horizon deformation directions. We add matrix vectors of uE and uN. The new matrix is sampled down. We normalize the up matrix and gain the right size of arrows. The size of the arrow shown in the map is defined as follows:

$$d = k \times r \times \frac{d_0}{uZ_{max}} \tag{4}$$

where d_0 represents the horizon deformation, uZ_{max} represents maximum deformation of the up direction, r represents the size of one pixel of uZ map, and k represents scaling.

Finally, we add the arrows to the uZ map to represent the horizontal displacements and do an inverse process to wrap the LOS deformation (Fig. 3 g, h). Due to the limitation of the resolution of resultant maps, we ensure that each map is within 5 cycles. Wrapping is described in Fig. 4. We input ascending or descending deformation value $V = [v_1, v_2, \cdots v_i]^T$ into the program, and then obtain the new wrapping value $V' = [v_1', v_2', \cdots v_i']^T$.

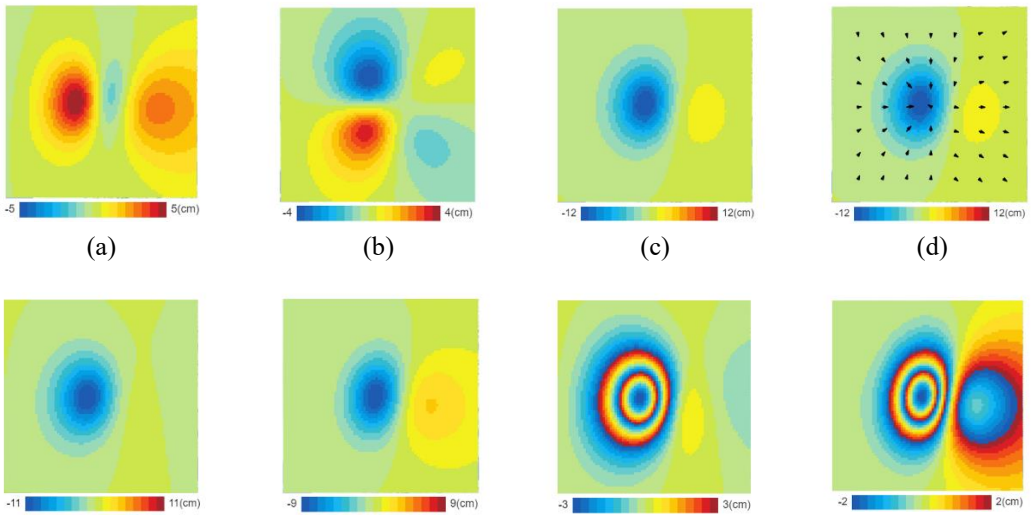

(a) (b) (c) (d)

(e) (f) (g) (h)

Figure 3. All seismic deformation maps. From (a) to (h), there are uE, uN, uZ, 3D, ascending, descending, wrapping ascending, and wrapping descending maps, respectively.

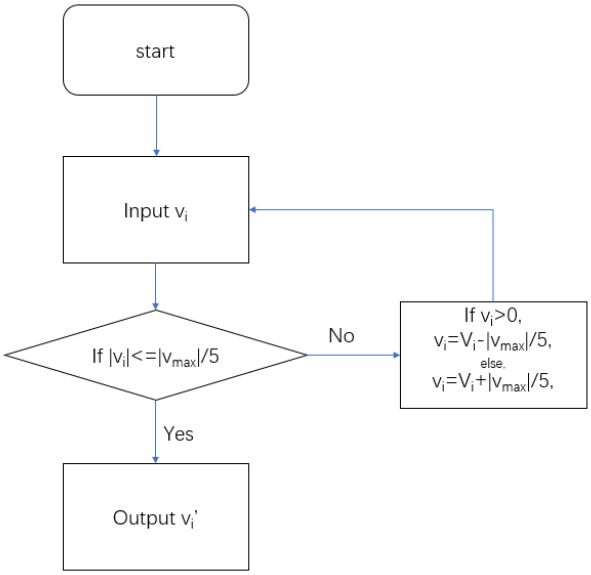

Figure 4. Wrapping processing.

To support the automatic framework, we import certain significant plugins. Primarily, the forward modeling generates the surface deformation matrix in kilometers so that we register the deformation matrix into the Mercator coordinate system, which is the reference coordinate system of Leaflet. Moreover, earthquakes of different magnitudes can affect the surface of different ranges. A stronger earthquake will cause larger damage. Therefore, we automatically visualize seismic deformation according to different magnitudes of earthquakes using spatial data fusion technology. The visible region is a square. The relationship between the length of a side R and the magnitude M_0 can be described as follows:

$$R = \begin{cases} 50 & 5.5 \le M_0 < 7 \\ 100 & 7 \le M_0 < 8 \\ 300 & 8 \le M_0 < 8.6 \\ 600 & 8.6 \le M_0 < 9 \\ 800 & 9 \le M_0 < 9.3 \\ 1500 & M_0 \ge 9.3 \end{cases} \tag{5}$$

4. Results and discussion

We implement the WebGIS platform, namely QuickDeform at www.insar.com.cn, as described in Section 3, followed by discussion.

4.1 Data sets and processing

The proposed framework automatically accesses the earthquake source parameters using the focal mechanism from the USGS-NEIC, which provides real-time or near real-time data on Earth observation. The USGS-NEIC filters significant earthquakes that can affect human activities. In addition, the framework focuses on earthquakes whose magnitude is larger than 5.5. The framework collects the raw data of the significant earthquake and stores these data (Table 2) into the database.

Table 2. Sample data of the structured database (note: DT for Datetime, Lat. For Latitude, Lon. for Longitude and Mag. For Magnitude)

ID	Title	DT	Lat.	Lon.	Mag.	Depth	Strike	Dip	Rake
10	M 6.6- 50km S of Tanaga Volcano, Alaska	2018-08-05 11:46:37 UTC	-8.287	116.452	6.9	31	269	62	88
11	M 6.4 - 252km SE of Iwo Jima, Japan	2018-08-16 18:22:52 UTC	23.441	143.341	6.4	21.5	351	68	100

4.2 Platform design

Due to the development of information and communication technology, GIS has made significant progress from a system tool to service and science. It has become a ubiquitous tool for various applications, ranging from transportation, emergency evacuation, navigation, and urban planning. WebGIS or mobile GIS is probably the most widely used GIS tool in many fields. There are many earthquake early warning systems based on WebGIS, such as ShakeMap and ShakeAlert (Böse et al., 2014). Compared with traditional desktop GIS, WebGIS has obvious advantages (Fu & Sun, 2010; Lagmay et al., 2017), including 1) Globalization, as these platforms can be assessed from computers or mobile devices; 2) The simultaneous access by a large number of users is supported, whereas traditional desktop GIS can only be used by one user at a time; 3) Better cross-platform-ability. HTML-based WebGIS can usually support different systems (e.g., Microsoft Windows, Linux, and Apple MacOS; 4) Easy to use and develop. WebGIS can be used by wide audiences, including users who know nothing about GIS. And the open-source package allows developers to easily customize their applications; 5) Unified update. This ease of maintenance makes the WebGIS ideal for providing real-time data; 6) No need for data transfer. Users can browse and operate the maps without downloading them.

The technical aspects of this real-time integration seismic deformation framework are driven by two main technologies. The front-end is an open-source JavaScript library for interactive mapping called Leaflet (Leaflet, 2018), and the back-end is Django (Django, 2018) which is a high-level Python Web framework. Leaflet can easily integrate different kinds of base-maps, including Google Maps, Microsoft Maps, OpenStreetMap (OSM), Stamen, and ESRI. Because of the simple structure of the raw data, we utilize MySQL (MySQL, 2018), which is open-source and light as the database of the platform. Likewise, it has a community that provides hundreds of powerful and convenient plugins, such as compass, legend and sidebar. Fig. 5 shows the structure of the platform.

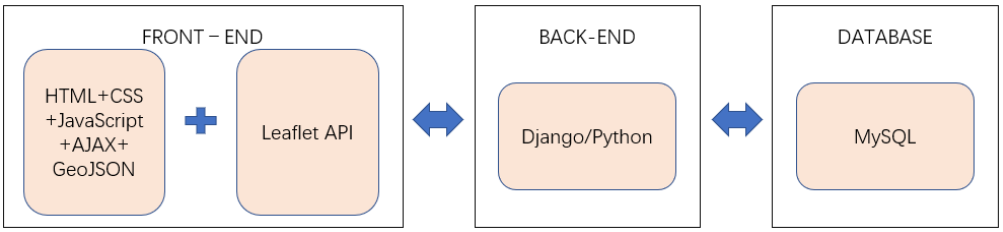

Figure 5. Architecture of QuickDeform platform

For front-end, except for the basic techniques HTML, CSS, and JavaScript, we mainly utilize Asynchronous JavaScript and XML (AJAX) technology and GeoJSON format. AJAX is a set of Web development techniques using several web technologies on the client-side to create asynchronous Web

applications. It can read data from a web server after a web page has loaded, and then send the data to a web server in the background and update a web page without reloading the page (Luan & Zhu, 2006). In addition, GeoJSON is one of the many geographic data structure encoding formats based on JavaScript Object Notation (JSON) (for more information, please refer to http://geojson.org).

4.3 QuickDeform

In this platform, visualization is an important part because the deformation map should be adaptive to the WebGIS platform and it should be friendly and readable to users. Therefore, we choose the basic color bar and utilize a fixed range of colors to visualize "forward", "reverse", and "zeroth" deformations. We fix the middle of the color bar (i.e., green) to represent zero deformation. Red represents forward deformation whereas blue represents reverse deformation. For example, for uE maps, red means deformation towards the east, whilst blue means deformation towards the west. Besides, we set the maximum scale of forward and reverse deformation to be the same. This color method adapts for visualization of uE, uN, uZ, Asc, Desc, Wrapping Asc, and Wrapping Desc maps.

The user interface of the real-time automatic generation of seismic deformation WebGIS is divided into three main parts. The first part is the automatic real-time earthquake deformation evaluation. Firstly, we can get the latest information on filtered earthquakes including different types of deformation maps, location, date-time, beachball, and focal mechanism. Secondly, the platform additionally provides the server with which the users can customize parameters to simulate seismic deformation. Thirdly, users can search recent earthquake counterpart information as the platform keeps the latest information. Furthermore, we add other useful layers into the platform. Because of the close connection between faults and earthquakes, we add global plate boundary data and main faults around China. Moreover, given that there is no surface deformation in the sea, if the impact of the earthquake is partly in the sea we add the global coastlines layer into the quick deform platform and users can easily distinguish land and sea. To make it easier to view base-map and surface deformation, we add the dragging slider, and users can adjust the transparency of the surface deformation layer to a suitable degree. According to the user's requirement, they can choose different types of base-maps, including Grayscale, Streets, Outdoors, Satellite, and Terrain according to their requirement.

We designed and developed an open-source WebGIS-based integration of seismic deformation real-time disaster evaluation framework to help seismologists, rescue workers, and even the public being informed about the seismic hazard. The platform is online, which grants access to everyone. As shown in Fig. 6, the designed user interface is compact, friendly, and readable to amateur users. When designing the user interface, we tend to use the style of the original Leaflet library. The platform has basic map elements such as map scale, legend and location function. However, it does not present further functions such as the adjustment of the transparency of layers, which is able to realize every effected area's deformation.

The main layer control panel is switched by the first button in the upper left corner of UI. The layer control panel (Fig. 6) is divided into three main parts: base-maps, deformation maps, and other layers. The base-maps are readily available and collected by Leaflet. All deformation maps and other layers are stored as GeoJSON files that can be easily visualized by the Leaflet engine.

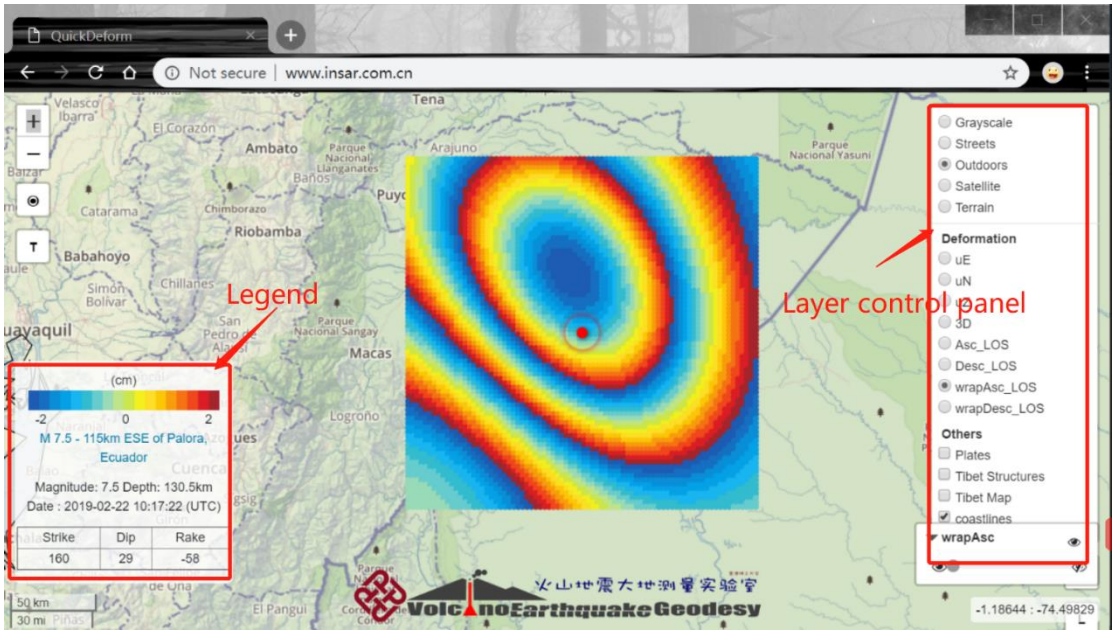

Figure 6. Online version of the real-time automatic generation of coseismic ground deformation platform distribution browser. Window displays the newest significant earthquake deformation in the eastern direction. In the lower-left corner of UI, there is a map scale, and above the map scale is the legend which records color bar, basic information of earthquake, and further information link (provided by the USGS). In the lower right corner of UI, there are a transparency sidebar and query coordinate control that follows the mouse in real-time. In addition, there are some buttons that control other panels on the upper two sides. The layer controller panel. From top to bottom, the main parts are respectively base-maps, latest seismic deformation maps, and other layers.

For the other functions, the side control panel (Fig. 7), which is switched by the second button in the upper left corner, can query recent significant earthquakes and customize the seismic parameters. Users can submit customized seismic parameters to the web server and gain corresponding deformation maps. For querying recent significant earthquakes, users can select the title of earthquakes and access data from the database, and basic information of earthquakes can be displayed in the custom panel. The color bar, location button, and transparency tools for these layers are different from what has been mentioned before. They are in the side control panel so that users can more easily compare the latest deformation maps with seismic deformation maps customized by users or recent seismic deformation maps.

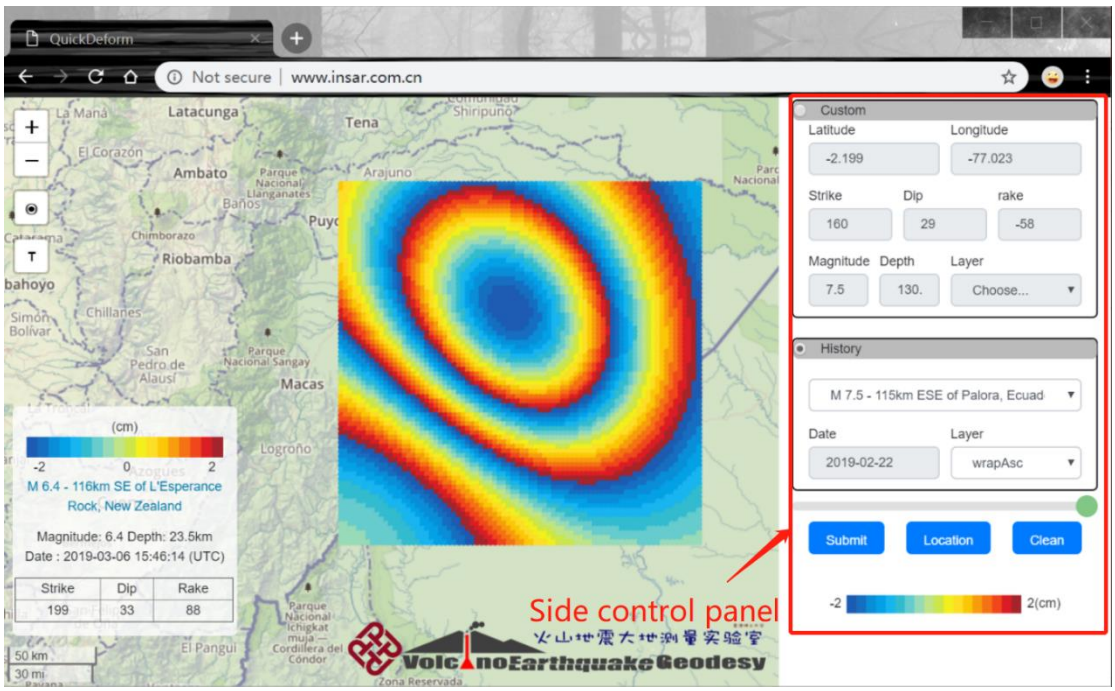

Figure 7. Side control panel. There are custom and history areas, as well as an own color bar and transparency tool in this panel.

Notably, although we need to obtain the focal mechanism that should be calculated and provided by the USGS-NEIC after the earthquake, the platform is able to get deformation results within 2 min after the data is released.

There is a discussion for nodal planes. When an earthquake happens, the USGS-NEIC provides two nodal planes, out of which, only one will suit the earthquake; however, it only can be judged by humans. In the experiments, we find that the seismic deformation from the two nodal planes parameters are similar. In this study, we select an earthquake that happened in Alaska on November 30, 2018. The main parameters are in Table 3. For further experiments, we compare the results of two different nodal planes. We only display the wrapping descending maps (Fig. 8) of this experiment. The two sets of nodal plane parameters are in Table 4. We find that the surface seismic deformation patterns that resulted from the two sets of nodal plane parameters are similar so that we only collect parameters of plane 1.

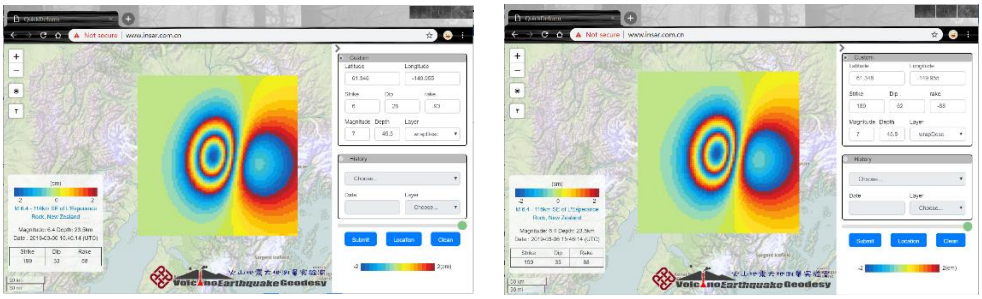

(a) (b)

Figure 8. (a) Wrapping descending map which is resulted from plane 1. (b) Wrapping descending map which is resulted from plane 2.

Table 3. Main parameters of the 2018 Mw 7.0 Alaska Earthquake

Magnitude	Depth(km)	Strike (°)	Dip (°)	Rake (°)
7.0	45.5	6	28	-93

Table 4. Nodal Plane of the 2018 Mw 7.0 Alaska Earthquake

Plane	Strike (°)	Dip (°)	Rake (°)
NP1	6	28	-93
NP2	189	62	-88

4.4 Discussions

For an emergency response system, response time is a very important variable. Herein, we test response information for 50 earthquakes. Although the focal mechanism is released by USGS-NEIC and the average processing time of the platform is 11.94 s, we cannot publish resultant maps after approximately 11.94 s. Generally speaking, when an earthquake occurs, USGS-NEIC can release basic information of the earthquake, such as depth, magnitude and coordinates, within seconds. However, as a crucial portion of the forward model, the focal mechanism is not released with basic information. Depending on the location and size of the earthquake, the release time of the focal mechanism is different. We have selected several typical earthquakes for comparison (Table 5).

Table 5. Sample earthquakes of focal mechanism release time

Name	Earthquake time	Focal mechanism time	Magnitude
8km S of Indios, Puerto Rico	2020-01-07 08:24 UTC	2020-01-07 08:45 UTC	6.4
13km SSE of Indios, Puerto Rico	2020-01-06 10:32 UTC	2020-01-06 11:20 UTC	5.8
182km W of Port Hardy, Canada	2019-12-25 03:36 UTC	2019-12-25 04:44 UTC	6.3
3km SW of Lejanias, Colombia	2019-12-24 19:03 UTC	2019-12-24 21:17 UTC	6.0
5km NE of Fall City, Washington	2019-12-19 03:10 UTC	NULL	3.4

Table 5 shows that the release time of the focal mechanism is uncertain. Even for several small earthquakes, USGS-NEIC does not provide the focal mechanism. Due to specific reasons, the release time of the focal mechanism of significant earthquakes is generally around tens of minutes. Because the seismic station network has an uneven distribution, the distance from the seismic center to the seismic station varies. Certainly, earthquake energy is also important (for more information, please refer to https://earthquake.usgs.gov/). Therefore, the response time of QuickDeform is approximately 5–10 min with sleep time. However, we cannot ensure the release time of the focal mechanism. Therefore, the time between the earthquake time and the release of resultant maps is variable. However, it is still more timely than InSAR data. For instance, we published the 2020 Mw Puerto Rico earthquake on January 7, 2020, approximately at 9 o'clock (UTC). In contrast, the fastest InSAR data was posted on Twitter on January 9, 2020 (https://twitter.com/EricFielding/status/1215525629409579009) (Hicks, 2019).

ShakeMap (USGS-NEIC) QuickDeform

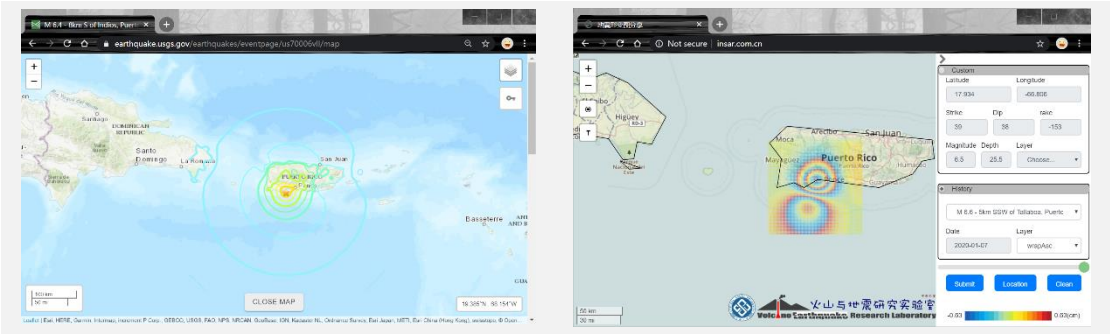

Figure 9. QuickDeform and ShakeMap. ShakeMap defines the maximum ground motion and shaking intensity is VII for this earthquake. QuickDeform can present the deformation of each pixel in centimeter.

We compare QuickDeform with ShakeMap using the 2020 Mw 6.5 Puerto Rico earthquake (Fig. 9). ShakeMap divides all the results into 10 levels. It provides rough equation lines of shaking intensity, and they have a larger visual range. In contrast, QuickDeform has more detailed surface deformation in the same region. And the results are in centimeters. QuickDeform does not need ShakeMap's visual range, because the effect of the exterior is small enough to be negligible.

We also compare several estimated surface deformations with real InSAR data. We only display the typical estimated surface seismic deformation that happened in Iran, in 2017. Chen et al. (2018) generated relatively complete ascending and descending orbit coseismic ground deformation maps associated with the 2017 Mw 7.3 Sarpol Zahāb earthquake. The main parameters are in Table 6. By comparing our synthetic InSAR deformation maps with Chen's model predictions, we can easily conclude that the estimated deformation map shows good agreement with real data (Fig 10). The result of QuickDeform is smoother. Fig 9 shows that the maximum deformation is approximately 60 cm and the maximum deformation of QuickDeform is approximately 50 cm. Because QuickDeform is a general emergency response platform that can publish every significant earthquake and deformation results are difficult to estimate for diverse earthquakes, the quantitative analysis of the results of only one or several earthquakes is not accurate. Compared to the real InSAR deformation, results of QuickDeform are consistent in magnitude, but the accuracy needs to be improved.

Table 6. Main parameters of the 2017 Mw 7.3 Sarpol Zahāb earthquake

Magnitude	Depth(km)	Strike (°)	Dip (°)	Rake (°)
7.3	15	351	15	135

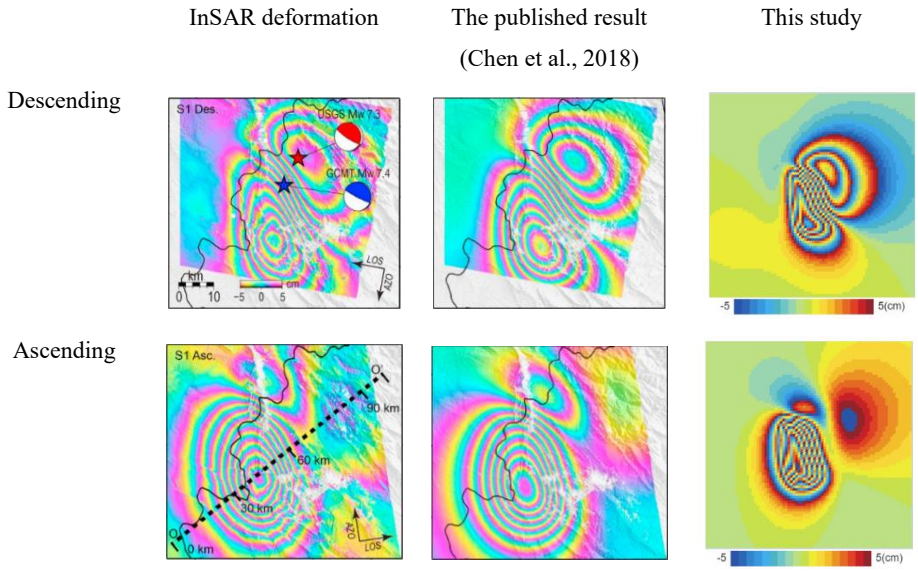

Figure 10. Deformation maps overall agree with InSAR deformation maps from the descending and ascending Sentinel-1 data and joint inversion slip model presented by Chen et al. (2018).

5. Conclusions

Earthquake evaluation and response have been examined with various monitoring methods. The rapid development of social media enables earthquake warnings to widely spread among the public. However, further profound analysis and timely information can enable researchers to quickly grasp the earthquake mechanism. Most studies cannot simultaneously consider timeliness and practicality. In this study, we make some significant contributions to the literature on automatic near real-time seismic deformation evaluation and response. We develop a framework based on near real-time data, fault model, and empirical equations and automatically visualize seismic deformation maps on WebGIS. Moreover, it is available to the public as an open-source (https://github.com/zhaorui-homepage/QuickDeform) platform (www.insar.com.cn) which is useful for seismic studies and rescue. The results of the platform can be published within dozens of minutes to an hour. In addition, the deformation map is reasonably consistent with the real InSAR data. Although the platform does not publish deformation maps in real-time, the near real-time and more accurate seismic deformation analysis can still provide profuse information.

Acknowledgments

We are grateful to the editor and anonymous reviewers for their insightful suggestions to significantly improve the quality of this paper. This research is partly supported by the Hong Kong Polytechnic University project (no.1-ZVN6), by the National Natural Science Foundation of China (No. 41804015) and by the National Key R&D Program of China (No. 2019YFC1509205).

References

Allstadt, K. E., Jibson, R. W., Thompson, E. M., Massey, C. I., Wald, D. J., Godt, J. W., & Rengers, F. K. (2018). Improving near-real-time coseismic landslide models: Lessons learned from the 2016 Kaikōura, New Zealand, earthquake. *Bulletin of the Seismological Society of America*.

Atkinson, G. M., & Boore, D. M. (1998). Evaluation of models for earthquake source spectra in eastern North America. *Bulletin of the Seismological Society of America*, 88(4), 917-934.

Balzter, H., Cole, B., Thiel, C., & Schmullius, C. (2015). Mapping CORINE land cover from Sentinel-1A SAR and SRTM digital elevation model data using random forests. *Remote Sensing*, 7(11), 14876-14898.

Beeler, N. M., Lockner, D. L., & Hickman, S. H. (2001). A simple stick-slip and creep-slip model for repeating earthquakes and its implication for microearthquakes at Parkfield. *Bulletin of the Seismological Society of America*, 91(6), 1797-1804.

Blaser, L., Krüger, F., Ohrnberger, M., & Scherbaum, F. (2010). Scaling relations of earthquake source parameter estimates with special focus on subduction environment. *Bulletin of the Seismological Society of America*, 100(6), 2914-2926.

Böse, M., Allen, R., Brown, H., Gua, G., Fischer, M., Hauksson, E., ... & Maechling, P. (2014). CISN ShakeAlert: An earthquake early warning demonstration system for California. In Early warning for geological disasters (pp. 49-69). Springer, Berlin, Heidelberg.

Chen, K., Xu, W., Mai, P. M., Gao, H., Zhang, L., & Ding, X. (2018). The 2017 Mw 7.3 Sarpol Zahāb Earthquake, Iran: A compact blind shallow-dipping thrust event in the mountain front fault basement. *Tectonophysics*, 747, 108-114.

Cronin, V. (2010). A primer on focal mechanism solutions for geologists. *Science Education Resource Center, Carleton College.*

Django Software Foundation and individual contributors. (2005) Available: https://www.djangoproject.com/

Douglas, J., & Edwards, B. (2016). Recent and future developments in earthquake ground motion estimation. *Earth-Science Reviews*, 160, 203-219.

Fialko, Y., Simons, M., & Agnew, D. (2001). The complete (3-D) surface displacement field in the epicentral area of the 1999 Mw7. 1 Hector Mine earthquake, California, from space geodetic observations. *Geophysical Research Letters*, 28(16), 3063-3066.

Fu, P., & Sun, J. (2010). *Web GIS: principles and applications*. Esri Press.

Giardini, D., Grünthal, G., Shedlock, K. M., & Zhang, P. (1999). The GSHAP global seismic hazard map. *Annals of Geophysics*, 42(6).

Goldstein, R. M., Zebker, H. A., & Werner, C. L. (1988). Satellite radar interferometry: Two-dimensional phase unwrapping. *Radio science*, 23(4), 713-720.

Hicks, S. P. (2019). Geoscience analysis on Twitter. Nature Geoscience, 12(8), 585-586.

Hough, S. E. (2016). *Predicting the unpredictable: the tumultuous science of earthquake prediction*. Princeton University Press.

Hu, J., Li, Z. W., Ding, X. L., Zhu, J. J., Zhang, L., & Sun, Q. (2012). 3D coseismic displacement of 2010 Darfield, New Zealand earthquake estimated from multi-aperture InSAR and D-InSAR measurements. *Journal of Geodesy*, 86(11), 1029-1041.

Hu, J., Li, Z., Zhu, J., Ren, X., & Ding, X. (2010). Inferring three-dimensional surface displacement field by combining SAR interferometric phase and amplitude information of ascending and descending orbits. *Science China Earth Sciences*, *53*(4), 550-560.

Kohler, M.D., Smith, D.E., Andrews, J., Chung, A.I., Hartog, R., Henson, I., Given, D.D., de Groot, R. and Guiwits, S., (2020). Earthquake Early Warning ShakeAlert 2.0: Public Rollout. *Seismological Research Letters*.

Lacassin, R., Devès, M., Hicks, S., Ampuero, J.P., Bossu, R., Bruhat, L., Wibisono, D., Fallou, L., Fielding, E., Gabriel, A.A. and Gurney, J., (2019). Rapid collaborative knowledge building via Twitter after significant geohazard events.

Lagmay, A. M. F. A., Racoma, B. A., Aracan, K. A., Alconis-Ayco, J., & Saddi, I. L. (2017). Disseminating near-real-time hazards information and flood maps in the Philippines through Web-GIS. *Journal of Environmental Sciences*, 59, 13-23.

Leaflet 1.2.0. (2017) Available: https://leafletjs.com/

Lin, J.L., Chen, Y.H., Hsiao, K.H. and Huang, J.F., (2019). Exploration of Ancient Machinery: From Reconstruction Research to Exhibition and Science Education. In *Explorations in the History and Heritage of Machines and Mechanisms* (pp. 134-143). Springer, Cham.

Liu, X., & Xu, W. (2019). Logarithmic model joint inversion method for coseismic and postseismic slip: Application to the 2017 Mw 7.3 Sarpol Zahāb earthquake, Iran. Journal of Geophysical Research: Solid Earth, 124, 12,034–12,052. https://doi.org/10.1029/2019JB017953.

LUAN, S. P., & ZHU, C. Q. (2006). A new mode of WebGIS development based on Ajax [J]. *Engineering of Surveying and Mapping*, 6, 008.

Okada, Y. (1985). Surface deformation due to shear and tensile faults in a half-space. Bulletin of the seismological society of America, 75(4), 1135-1154.

Okada, Y. (1992). Internal deformation due to shear and tensile faults in a half-space. Bulletin of the seismological society of America, 82(2), 1018-1040.

Simons, M., Fialko, Y., & Rivera, L. (2002). Coseismic deformation from the 1999 M w 7.1 Hector Mine, California, earthquake as inferred from InSAR and GPS observations. *Bulletin of the Seismological Society of America*, 92(4), 1390-1402.

Standard, F. (1996). Telecommunications: Glossary of teikolecommunication terms. *Retrieved January*, *15*(2004), 69-72.

Stramondo, S., Bozzano, F., Marra, F., Wegmuller, U., Cinti, F. R., Moro, M., & Saroli, M. (2008). Subsidence induced by urbanisation in the city of Rome detected by advanced InSAR technique and geotechnical investigations. *Remote Sensing of Environment*, 112(6), 3160-3172.

United States Department of the Interior, United States Geological Survey. (2011). Available: https://pubs.usgs.gov/fs/2011/3021/index.html

Wald, D. J., Quitoriano, V., Heaton, T. H., Kanamori, H., Scrivner, C. W., & Worden, C. B. (1999). TriNet "ShakeMaps": Rapid generation of peak ground motion and intensity maps for earthquakes in southern California. *Earthquake Spectra*, 15(3), 537-555.

Wald, D.J., Worden, C.B., Thompson, E.M. and Hearne, M., (2019). Earthquakes, ShakeMap. Encyclopedia of Solid Earth Geophysics, pp.1-6.

Watson, K. M., Bock, Y., & Sandwell, D. T. (2002). Satellite interferometric observations of displacements associated with seasonal groundwater in the Los Angeles basin. *Journal of Geophysical Research: Solid Earth*, 107(B4).

Wu, Y. M., Shin, T. C., & Tsai, Y. B. (1998). Quick and reliable determination of magnitude for seismic early warning. *Bulletin of the Seismological Society of America*, 88(5), 1254-1259.

Xu, W., Wu, S., Materna, K., Nadeau, R., Floyd, M., Funning, G., ... & Bürgmann, R. (2018). Interseismic ground deformation and fault slip rates in the greater San Francisco Bay Area from two decades of space geodetic data. *Journal of Geophysical Research: Solid Earth*, 123(9), 8095-8109.

Xu, W., Dutta, R., & Jónsson, S. (2015). Identifying active faults by improving earthquake locations with InSAR data and Bayesian estimation: the 2004 Tabuk (Saudi Arabia) earthquake sequence. *Bulletin of the Seismological Society of America*, 105(2A), 765-775.

Xu, W., Feng, G., Meng, L., Zhang, A., Ampuero, J. P., Bürgmann, R., & Fang, L. (2018). Transpressional rupture cascade of the 2016 Mw 7.8 Kaikoura earthquake, New Zealand. *Journal of Geophysical Research: Solid Earth*, 123(3), 2396-2409.